J. Fluid Mech. (2000), *vol.* 402, *pp.* 137–162. Printed in the United Kingdom

Experimental probability density functions of small-scale fluctuations in the stably stratified atmosphere

By JEAN-RÉMI ALISSE AND CLAUDE SIDI

Service d'Aéronomie du CNRS, BP3, 91371 Verrières-le-Buisson, France

(Received 9 March 1998 and in revised form 5 August 1999)

Small-scale random fluctuations of atmospheric variables are ubiquitous dynamical components in the stable, free atmosphere. There, within the $O(1–10\,\mathrm{m})$ vertical wavelength band, spectra of temperature and horizontal velocity often follow either a $m^{-5/3}$ or a m^{-3} power law, m being the vertical wavenumber. Using high-resolution vertical profiles obtained by balloon-born instrumentation in the troposphere and stratosphere, we determine experimental probability density functions (PDFs) of velocity and temperature fluctuations in the spectral band (2–20 m) within atmospheric layers which follow one or the other spectral law. PDFs of such band-filtered fluctuations of temperature and velocities (horizontal and vertical) are estimated within 101 seemingly homogeneous atmospheric layers. It appears that PDFs of horizontal velocity fluctuations, once normalized by their r.m.s. values, do collapse towards two significantly different regimes depending upon the spectral law followed in the wavelength band considered. On the other hand, temperature fluctuation PDFs are shown to be close to each other in both regimes. All these PDFs show close-to-exponential tails. Their high kurtosis appears to be mainly related to intermittency of the fluctuations fields, though marginal influence of residual inhomogeneity of the selected layers may be suspected. These results are compared with published results of laboratory and numerical experiments. We wish to emphasize the unexpected non-Gaussian character of these PDFs.

1. Introduction

The study of the probability density functions (PDFs) of fluctuations in turbulence has received a renewed interest in the last few years, from a theoretical (Pope 1985, 1994; Sinai & Yakhot 1989; Yakhot 1989; Ching 1993, 1996), numerical (Vincent & Meneguzzi 1991; Métais & Lesieur 1992; Jaberi *et al.* 1996; Ching & Tsang 1997) and experimental point of view. This interest is related to the intense research on intermittency of turbulent signals, which may be demonstrated by the shape of PDFs (Frisch 1995). Many of the experimental studies (Castaing, Gagne & Hopfinger 1990; Gollub *et al.* 1991; Jayesh & Warhaft 1991, 1992; Guilkey *et al.* 1997) deal with laboratory measurements, where temperature can be considered as a passive scalar. However, Castaing *et al.* (1989) published PDFs of temperature in a convective medium, this question being also adressed by Van Atta & Park (1972) in the planetary boundary layer. More recently, Thoroddsen & Van Atta (1992) published PDFs obtained in a strongly stratified wind tunnel. Results obtained in the planetary

boundary layer have already been published by Katul (1994), but limited to neutral or slightly-stratified flows.

We present below estimations of the PDFs of temperature and velocity small-scale fluctuations in the stable, clear, free atmosphere above the planetary boundary layer and up to the stratosphere. There, temperature is not a passive tracer and it may be shown that temperature fluctuations correspond to available potential energy (E_P) reservoirs, as pointed out by Phillips (1967). Energy exchanges between kinetic energy (E_K) and E_P reservoirs are expected to occur at all scales. Thus, specific connections between temperature and velocity fluctuations may be anticipated, with, possibly, some influence upon their respective PDFs.

Vertical profiles of temperature and velocities in the stable, free atmosphere usually show a sequence of layers with more or less intense small-scale activity. Assuming statistical homogeneity of small-scale fluctuations within definite layers, spectra of temperature, and horizontal and vertical velocities may be estimated. Within strong signal amplitude regions, these spectra often scale like $m^{-5/3}$ in the short-wavelength band, typically $O(1\text{–}10\,\mathrm{m})$, m being the vertical wavenumber, thus suggesting a close-to-inertial subrange, *à la Kolmogorov*. Somewhat less known is the fact that within calm (non-turbulent) layers the same spectra in the same spectral band often scale like m^{-3} down to the instrumental noise level (Sidi & Dalaudier 1989; Dalaudier *et al.* 1994*a*), except for the vertical velocity ones, which grow much slower towards larger scales. This spectral m^{-3} behaviour has been extensively studied since the sixties, and is usually associated with the presence of a stable vertical gradient of temperature. It is hence called the 'buoyancy subrange' (Lumley 1964; Phillips 1967). These two power laws are by far the most frequently encountered, and thus suggest that small-scale fluctuations mainly result from different dynamical regimes, termed hereafter 'turbulent' and 'calm'. Note that some layers ($\simeq 20\%$ of the analysed set) show a quite different spectral behaviour, with slopes ranging from -1 to -4 or with different slopes for the temperature and horizontal velocity spectra. The available data relative to these atypical situations are not sufficient to document them accurately. Therefore the analysis hereafter only refers to those layers such that both temperature and horizontal velocity spectra scale like $m^{-5/3}$ or m^{-3}.

PDFs are primary characteristics of fluctuating fields. Their study may give hints about some basic mechanisms, such as the intermittency, and help delineate differences between the two regimes. Thus, our main aim is to characterize and compare PDFs of atmospheric variables, estimated within layers showing either a $m^{-5/3}$ or a m^{-3} spectral power law at short vertical wavelengths, using vertical profiles measured in the atmosphere by balloon-born instrumentation. To compare the distributions, we use the Kolmogorov–Smirnov (KS) test. The basics of KS test and some discussion about its application in the present context may be found in the appendix. The atmospheric data used in this paper will be briefly presented in the next section. They have been obtained during four stratospheric balloons flights, during a field experiment called RASCIBA, held in 1990, and devoted to radar and scintillometer signals physics (Dalaudier *et al.* 1994*b*; Luce *et al.* 1995). We then present the layer selection process which mainly relies on detection of velocity small-scale activities. It includes the following steps: (i) detection of data sections with a minimum length around 200 m showing intense or weak activities within the velocity first difference profiles; (ii) delimitation of subsections with a nearly constant temperature gradient, in order to control the influence of stratification; (iii) check of the consistency of the temperature and velocity spectra; (iv) inspection of the apparent homogeneity of the filtered fluctuations profiles. One hundred and one calm or turbulent layers

have been delineated following these steps. The main dynamical characteristics of the two regimes are shown by estimating, within each layer, the gradient Richardson number Ri, the Thorpe length (Thorpe 1977) L_T, which may be considered as an index of overturnings, and the fluctuation variances. Briefly, turbulent (calm) layers have weaker (larger) Ri, significative (negligible) L_T, and close-to-isotropic (anisotropic) velocity fluctuations. Within turbulent layers, we also computed kinetic and available potential energy dissipation rates and the Lumley–Shur–Ozmidov scales as well. PDFs of normalized velocities and temperature fluctuations within these layers are then estimated and compared, using the Kolmogorov–Smirnov test. Horizontal velocity PDFs appear to collapse towards two significantly different ones depending upon the dynamical regime of the layer. On the other hand, normalized temperature fluctuation PDFs always appear very close to each other, whatever the dynamical regime. While turbulent vertical velocity PDFs also nearly collapse towards a single PDF, nearly identical to the turbulent horizontal velocity PDF, less distinct results are obtained for vertical velocities within calm layers. All these estimated PDFs are clearly non-Gaussian and show close to exponential long-extended tails. In the last section, we first discuss the main experimental uncertainties and show that they cannot qualitatively influence the PDF estimations. Since the high kurtosis and its increase with decreasing spatial scale of the turbulence are usually associated with intermittency (Yakhot 1989; Frisch 1995, p. 122), we test if these results are actually related to that phenomenon, or due to residual inhomogeneity of the selected layers. We show, using a heuristic argument, that inhomogeneity cannot account for all the high kurtosis observed. Then, we underline similarities and differences of the present results to those obtained by numerical simulations and laboratory experiments. We emphasize the close-to-exponential tails that we have observed, while stratified fluids numerical simulations (Métais & Lesieur 1992) and laboratory experiments (Thoroddsen & Van Atta 1992) show Gaussian tails. A tentative explanation relying upon the relative position of the spectral band considered with respect to the sources scale is suggested.

2. The data set

2.1. *Measurements and data processing*

The data discussed here have been obtained by balloon-born instrumented gondolas during the RASCIBA field experiment (Dalaudier *et al.* 1994*b*; Luce *et al.* 1995). Measurements were made aboard upwind-oriented gondolas, hung nearly 180 m below stratospheric balloons. The data have been obtained during four balloons ascents up to their ceilings (22–27 km) and during two descending parts of these flights, down to the tropopause. These flights are listed in table 1. The lower altitudes considered during the ascents correspond to the cloud upper limits. These flights occurred at night, passing through quite different meso- and synoptic-scale dynamical conditions: strong internal gravity wave activity during flights 14 and 15, extremely calm atmosphere during flight 16, strong tropopause jet during flight 19.

Instrumentation included fast-response cold-wire thermometers, a two-axis ionic anemometer (vertical and horizontal), a magnetometer, and a high-precision barometer, following the so-called 'differential sounding' methodology (Barat 1982). A brief sketch of the gondola is presented in figure 1. Some discussion about the significance of the upwind-oriented anemometry may be useful at this point. Assuming that the balloon closely follows the horizontal velocity of the air mass in which it is embedded, the anemometer data in the horizontal direction, $\Delta U(z)$, when combined with the

Flight reference	Type	Date	Altitude range (km)
14*A*	Ascent	19 Feb. 1990	5–25
15*A*	Ascent	20 Feb. 1990	3–25
15*D*	Descent	20 Feb. 1990	22–13
16*A*	Ascent	21 Feb. 1990	4–21
16*D*	Descent	22 Feb. 1990	21–12
19*A*	Ascent	1 Mar. 1990	4–25

TABLE 1. Balloon flights references.

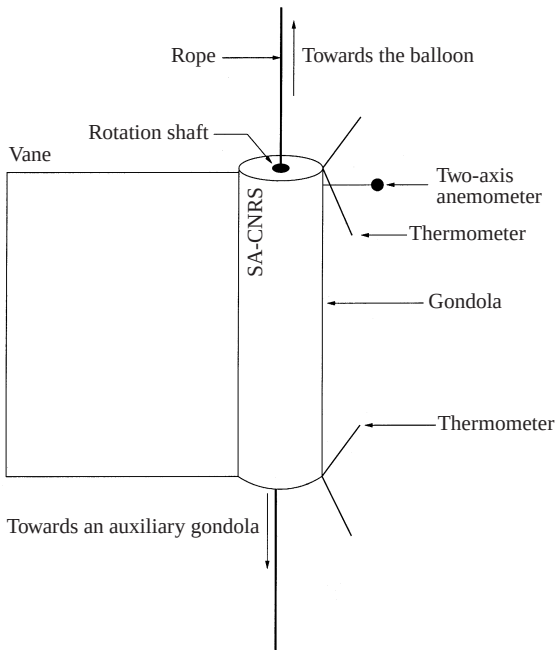

FIGURE 1. Sketch of the gondola. The dimension of the vane is around 1 m^2.

magnetometer data, give the relative horizontal velocity, $\Delta \boldsymbol{U}(z) = \boldsymbol{U}(z) - \boldsymbol{U}(z+h)$, where h is the balloon–gondola distance and $\boldsymbol{U}$ the air horizontal velocity. Within a factor h, these anemometer data may be interpreted as an estimation of the local shear, S at the altitude $z + h/2$, using

$$S(z + h/2) = \frac{1}{h}\Delta U(z). \tag{2.1}$$

It may be shown that the high-frequency content of these relative velocities only refers to the velocity fluctuations at the gondola level, as a result of the smoothing effects of both the large size ($O(20\,\mathrm{m})$) and the inertia of the stratospheric balloon (Barat 1982). Thus, the fluctuations of the anemometric signal, $U'(z)$, are the projections of the horizontal velocity fluctuations on the direction of the horizontal velocity shear at the altitude $z + h/2$.

The sampling rate (32 Hz) allows vertical resolutions ranging from about 10 cm to 20 cm, depending upon the balloon vertical velocity. This resolution and the sensor

sizes (a few cm) are well above the dissipation scales. Notice that, as a result of the balloon vertical velocity (about $6\,\mathrm{m\,s^{-1}}$ during the ascents, about $3\,\mathrm{m\,s^{-1}}$ during the descents), and the varying relative wind modulus and orientation at the gondola level (0–$6\,\mathrm{m\,s^{-1}}$), measurements are made along complex helical pathes with respect to the flow. We neglect this aspect and consider data resampled at equispaced vertical distances (0.2 m during the ascents, and 0.1 m during the descents). This approximation will be discussed in the last section. The velocity of gondolas with respect to the flow being much larger than the typical velocity fluctuations considered here, we apply the Taylor frozen-field hypothesis. Further details about the instrumentation may be found in Dalaudier *et al.* (1994*b*) and references therein.

Hereafter, the small-scale fluctuations we consider will be band-filtered data in the vertical wavelength band (2–20 m). We consider band-filtered data instead of increments in order to avoid contamination of small-scale fluctuation statistics by mesoscale vertical shears. This contamination results from two unavoidable characteristics of the atmospheric dynamics, i.e. (i) there is no scale separation between small and mesoscale dynamical components; (ii) the mesoscale energy spectra in the free troposphere and stratosphere scale like m^{-3} up to wavelengths of $O(10^3\,\mathrm{m})$, see e.g. Smith, Fritts & VanZandt (1987), Sidi *et al.* (1988). Consequently, short vertical distance increments are always significantly influenced by varying mesoscale vertical shears.

The wavelength band has been chosen in such a way that it allows statistical properties of the two dynamical regimes (with a $m^{-5/3}$ or m^{-3} spectrum) to be compared in the same wavelength band. The shorter wavelength limit (2 m) was chosen to minimize noise contributions to the fluctuations statistics. The larger one (20 m) results from an experimental fact: $m^{-5/3}$ spectra, when present in stratospheric data, are scarcely observed at wavelengths larger than 20 m. Then, temperature and horizontal velocity spectra grow steeper towards the mesoscale range, following the m^{-3} scaling. Moreover, the transition between these spectral domains occurs close to the Lumley–Shur–Ozmidov scale ($L_b = 2\pi(\epsilon/N^3)^{1/2}$, ϵ is the dissipation rate, N is the Brunt–Väisälä frequency). In the stratosphere, L_b is of the order 20 m within turbulent layers, and much larger in the troposphere (Hocking 1985 and the present article).

Thus, starting from the original time recordings, data processing includes the following successive steps:

(i) data resampling at equally spaced vertical distances (cubic-spline interpolation);

(ii) withdrawal of a broken-line rough trend (to remove most of the low-wavenumber components, see Frankignoul 1974 or Press *et al.* 1994, p. 552);

(iii) filtering using classical band-pass FIR filters (Rabiner & Gold 1975);

(iv) undersampling of the resulting series in accordance with the new high-wavenumber cut-off: one sample per metre.

2.2. *Selection of layers*

We present in figures 2 and 3 series of temperature T and anemometric signals ΔU, together with zooms at different scales. Also plotted are the profiles of first differences δT and δU, which helps delineate more clearly the limits of every layer. The selection of the data sections considered in § 3 proceeds as follows. First, a careful scrutiny of all the available data profiles allows one to eliminate a lot of short data subsections suspected to be contaminated by instrumental wakes (wakes of the balloon, or even of the gondola itself, in some cases of misalignements of the gondola

with the relative wind). While these data subsections only represent a few percent of the whole data set, they reduce somewhat the number of large, calm or turbulent layers available.

Then, using visual inspection of profiles of U', W', δU and δW, we delineate areas showing turbulent activity, clearly distinguishable from their surroundings, and areas with no turbulent activity. We emphasize that we consider here only the velocity fluctuation profiles. We chose this rule because turbulence, within the present data set, seemingly originates from some kind of dynamical instability. Estimations of the Thorpe lengths (see below) show that overturnings only occur at small, turbulent scales. Furthermore the sensitivity of T' fluctuation intensity to local variations of $\mathrm{d}T/\mathrm{d}z$ prevents T' profiles being used as reliable evidence of turbulence.

We can show (see the Appendix) that to have enough information to compute reliable statistical parameters of fluctuations in the wavelengths 2–20 m such as the PDFs, the depth of a layer should at least be around 200 m. Hereafter, we will hence consider only such layers, with the exception of a few thiner ones, as explained below. Note that many turbulent layers thinner than 200 m have been observed in the atmosphere, as already described (Barat 1982; Sato & Woodman 1982). We just cannot estimate statistically significant parameters from such thin layers, and have hence not included them in our study. Each selected layer is then restricted to (or split into) narrower one(s) with a nearly constant mean temperature gradient. The choice of constant temperature gradient layers is made to allow some 'control' over the stratification parameter which is of great importance in any stably stratified fluid. Obviously this procedure narrows the layers, as compared with the ones resulting from the inspection solely of velocity profiles. The few thinner layers retained correspond to subsections with constant temperature gradients within seemingly homogeneous layers.

These key steps leading to the selection of definite layers allow for apparent intermittency of the turbulent signal, for instance the occurrence of narrow, calm subsections within an otherwise strong amplitude section. Clearly, a visual examination cannot distinguish between intermittency of turbulence and narrow (depths 200 m) calm layers interleaved with turbulent ones. Then the decision relies upon the examination of the mesoscale gradient Richardson number $Ri = N^2/S^2$. Ri is usually not constant within a layer, mainly as a result of the varying shear (see figure 2). When its variations are weak enough, we consider that we observe intermittency. Examples of such a situation may be found in figures 2 and 3. This criterion, however, does not prevent wrong decisions and we must keep in mind that some statistical inhomogeneity of the selected layers may be responsible for some of the non-Gaussian shape of the PDF. We shall discuss this point further in § 5.1.

Next, we consider the spectra of U' and T' in the same data section and reject all sections where both spectra do not show the same scaling ($m^{-5/3}$ or m^{-3}). While turbulent sections ($-5/3$ slopes) within U' and T' profiles mostly correspond, such a correspondence is not always observed within calm sections. There, some T' spectra do not show any explicit spectral slope, but rather some kind of 'deck chair' pattern between a m^{-3} scaling at larger scale and the noise level. Note that we do not test the consistency of W' spectra with those of U': while these spectra, in the spectral band (2–20 m), are close to the horizontal velocity ones within turbulent layers, they may strongly differ within calm layers, showing weaker energies, thus demonstrating anisotropy of the velocity field.

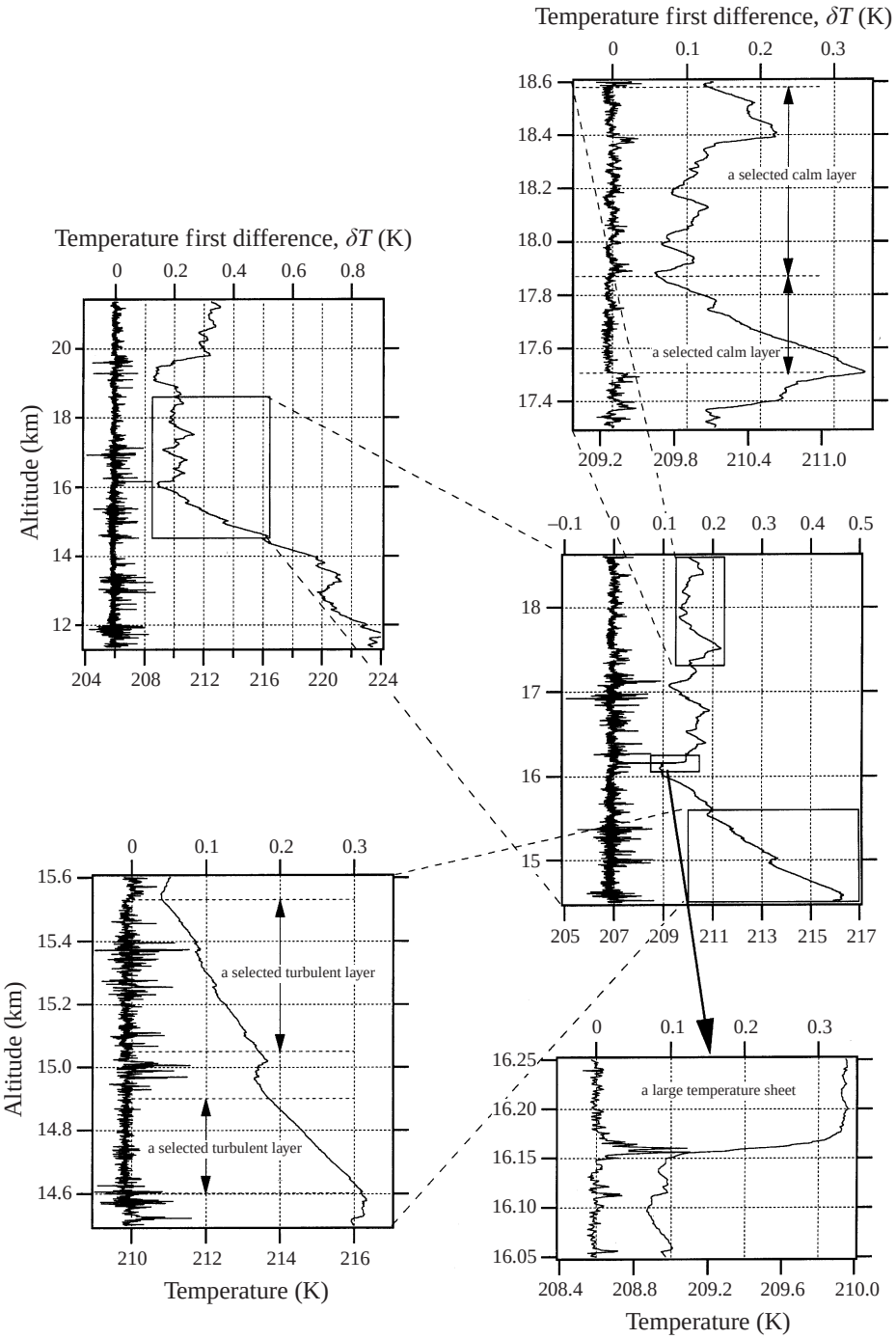

FIGURE 2. Successive enlargments of temperature vertical profiles, along with the corresponding first difference profiles (upper scales). To reduce noise contribution, the original data are low-pass filtered down to 2 m vertical wavelengths, and undersampled accordingly (1 m). The saw-toothed mesoscale structure of the temperature profile appears. Upper scales are the same in the three last enlargements, showing the varying small-scale activity. Characteristics of the referenced calm ($C15$ and $C16$) or turbulent ($T13$ and $T14$) layers may be found in table 3. A spectacular example of temperature sheets within a calm environment is shown (lower-right corner).

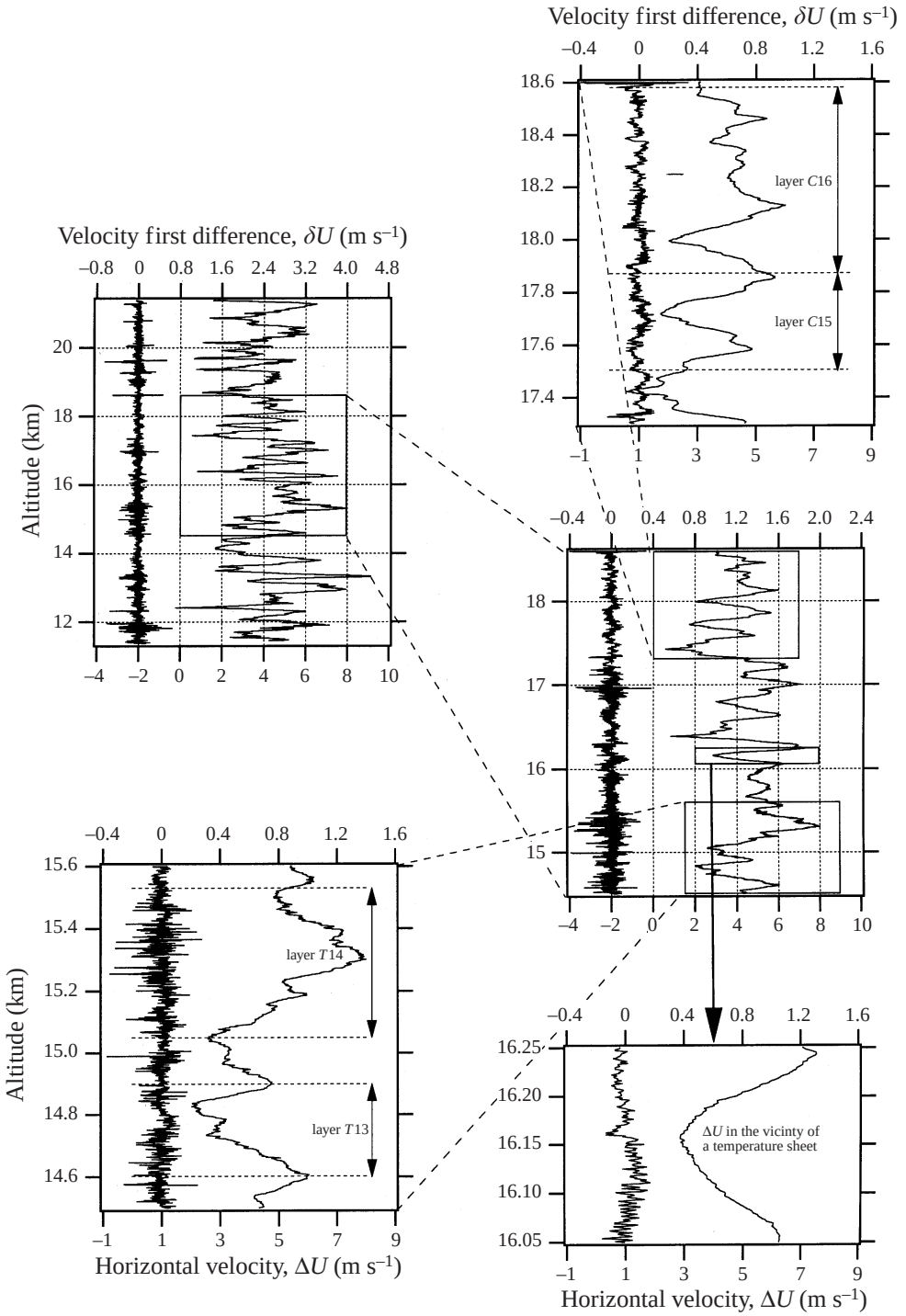

FIGURE 3. Same as figure 2 but for ΔU, the primary horizontal anemometric data (see text) and its first differences δU. Transitions between layers with different small-scale activity appears to be rather sharp. The ΔU profiles are shifted by half the balloon–gondola distance, such that they represent within a constant factor the horizontal velocity shear modulus at the right altitude.

Depth range (m)	150–399	400–599	600–799	800–999	$\geqslant 1000$	Total depth
Number of turbulent layers	32	4	1	0	1	10 830
Number of calm layers	45	14	3	1	0	20 010

TABLE 2. Distribution of the 101 layer depths.

3. Characterization of the layers set

We classify the layers as either turbulent or calm, according to their dynamical regime, as revealed by the power law followed by their U' and T' spectra: turbulent layers present a $m^{-5/3}$ spectra *à la Kolmogorov* and calm layers a m^{-3} spectra. 101 layers have been selected from the data set of the RASCIBA campaign, following the method described above, 38 turbulent and 63 calm. Table 2 displays the distribution of the depths of layers, and tables 3 and 4 give detailed characteristics of those layers referred to herein. A complete list of the characteristics of all 101 layers is available from the authors or the Journal of Fluid Mechanics Editorial Office. Typical U' and T' spectra from both regimes are shown in figure 4 (layers $C16$ and $T18$ in tables 3 and 4). We recall that, owing to the effective sensor pathes with respect to the flow, the U' spectra are neither strictly transverse nor longitudinal. We emphasize that, in both dynamical regimes, the energies found vary strongly from one layer to the next, presumably depending upon the mean local dissipation rates and stratification encountered.

Within each layer, we computed some pertinent dynamical parameters, namely the Brunt–Väisälä frequency N^2, a mean shear of horizontal velocity $\overline{S}$ and the corresponding gradient Richardson number $Ri = N^2/\overline{S^2}$. Since the shear S is variable inside each layer, Ri is computed using a mean $\overline{S}$ averaged over the layer. Figure 5 shows a scatter plot of N^2 and $\overline{S^2}$ for all the layers. Clearly, turbulent layers are associated with weaker Ri than the calm ones. Interestingly, most calm layers also have not particularly large Ri, thus showing that the atmosphere is on the verge of instability. We also computed the variances within the spectral band considered, corrected from an estimated (hypothetical) white noise level. Figure 6 shows a scatter plot of $\overline{U'^2}$ and $\overline{W'^2}$. This figure demonstrates the fact that the velocity fluctuations are close to isotropic within turbulent layers, and anisotropic within most of the calm ones.

Then, we estimated the Thorpe length (Thorpe 1977), which is a measure of the importance of overturnings. Here we use the fact that potential temperature is a conservative property of the fluid particles, like the density in water. Thus, the Thorpe length L_T is estimated as the r.m.s. value of the fluid particle vertical displacements required in order that the resulting potential temperature profile be everywhere stable (F. Dalaudier, see Staquet & Sommeria 1996, p. 363). Figure 7 presents this length as a function of the stratification parameter.

Within turbulent layers, we also estimated the dissipation rates of kinetic energy ϵ_K and of available potential energy ϵ_P, and the Lumley–Shur–Ozmidov length $2\pi k_B^{-1}$, with k_B the buoyancy wavenumber defined as $(N^3/\epsilon_K)^{1/2}$. The two dissipation rates were deduced from the variances corrected for the noise level using classical isotropic formulae (Lilly *et al.* 1974). We took into account the effective oblique path with respect to the flow (see § 5) and used the transverse velocity formulae to estimate ϵ_K.

A selection of those characteristics are displayed in table 3. To get a rough idea of the dynamical characteristics of both regimes, we present in table 5 the mean values

Ref.	Flight	Altitude km	Width m	$\left\langle \frac{d\overline{U}_H}{dz} \right\rangle$ $s^{-1} \times 10^{-2}$	N^2 $s^{-2} \times 10^{-4}$	Ri	ϵ_K $W\,kg^{-1} \times 10^{-4}$	ϵ_P $W\,kg^{-1} \times 10^{-5}$	$\overline{U'^2}$ $m^2\,s^{-2} \times 10^{-3}$	$\overline{W'^2}$ $m^2\,s^{-2} \times 10^{-3}$	$\overline{T'^2}$ $K^2 \times 10^{-4}$	L_B m	L_T m
T_1	14*A*	5.8	400	1.6	1.5	0.53	0.27	0.32	1.7	1.9	0.33	24	3.6
T_{13}	15*D*	14.75	300	1.8	0.8	0.24	1.18	2.8	4.5	2.7	0.43	80	12
T_{14}	15*D*	15.25	480	3.2	2.1	0.20	1.7	2	5.3	4.0	1.4	46	5
T_{16}	15*A*	3.75	750	0.7	3.6	0.58	6.3	5.2	10	7.3	0.34	60	27
T_{18}	15*A*	6.62	1240	1.7	0.7	0.25	3.8	4.2	7	4.6	0.6	160	23
T_{33}	19*A*	7.6	570	1.1	0.50	0.42	5.9	4.17	8.2	6.9	0.26	256	19

TABLE 3. Physical and dynamical parameters for some of the turbulent layers.

Ref.	Flight	Altitude km	Width m	$\left\langle \frac{d\overline{U}_H}{dz} \right\rangle$ s^{-1} $\times 10^{-2}$	N^2 s^{-2} $\times 10^{-4}$	*Ri*	$\overline{U'^2}$ $m^2\,s^{-2}$ $\times 10^{-3}$	$\overline{W'^2}$ $m^2\,s^{-2}$ $\times 10^{-3}$	$\overline{T'^2}$ K^2 $\times 10^{-4}$	L_T m
C_9	14*A*	21	570	1.1	5.8	4.36	1.55	0.78	3.5	0.22
C_{15}	15*D*	17.7	370	2.08	2.63	0.60	0.79	0.08	0.13	1.0
C_{16}	15*D*	18.2	710	2.14	5.01	1.08	0.85	0.13	0.31	0.34
C_{22}	16*A*	5.35	750	0.62	1.0	2.70	0.77	0.72	0.05	2.4
C_{63}	15*A*	24.25	600	3.1	5.1	0.50	3.5	0.99	0.22	0.25

TABLE 4. Physical and dynamical parameters for some of the calm layers.

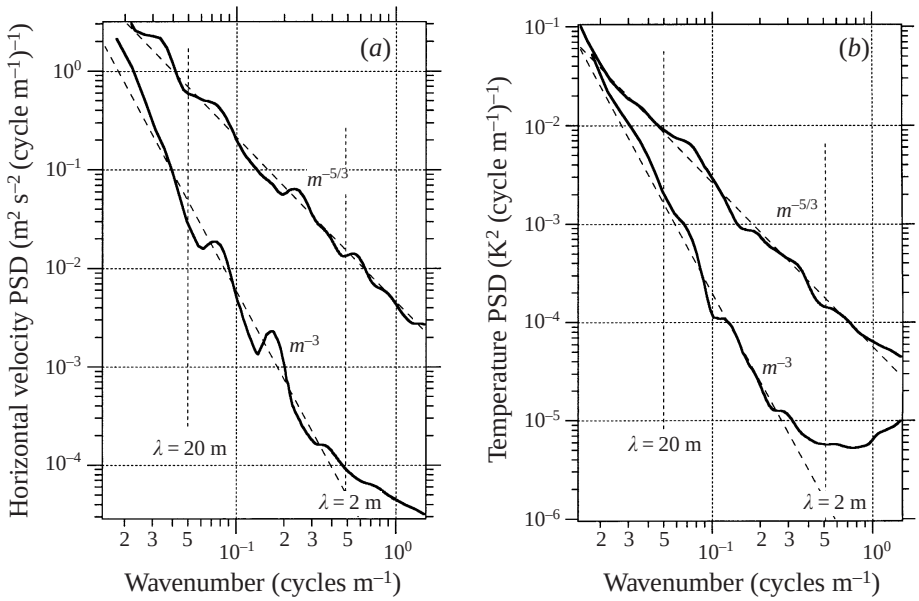

FIGURE 4. Spectra of (*a*) horizontal velocity and (*b*) temperature within typical turbulent (layer *T*18, number of degrees of freedom of the spectral estimation: 31) and calm layers (layer *C*16, number of degrees of freedom of the spectral estimation: 23). The spectra have been further smoothed with a window ensuring a constant $\delta m/m = 0.2$, where m is the vertical wavenumber. Note that for clarity, the turbulent spectra have been multiplied by a factor 5. The two dashed straight lines represent m^{-3} and $m^{-5/3}$ power laws.

of the parameters common to both regimes. It appears from those tables, and from figures 5, 6, 7, that the two regimes present somewhat different mean characteristics:

(i) the turbulent regime is nearly isotropic, associated with low *Ri* (usually lower than 1) and significative L_T;

(ii) the calm regime is frequently anisotropic, associated with weak or negligible L_T and larger *Ri* than the turbulent ones.

In spite of these mean differences, the two regimes overlap in figures 5, 6, 7. This may be interpreted as an indication of some ongoing time variations of the observed fields: we ignore at which step of their lifecycle we are measuring turbulent layers. In the same way, observed calm layers may be on the verge of instability: this could explain the not so high *Ri* values observed. On the other hand, these layers could

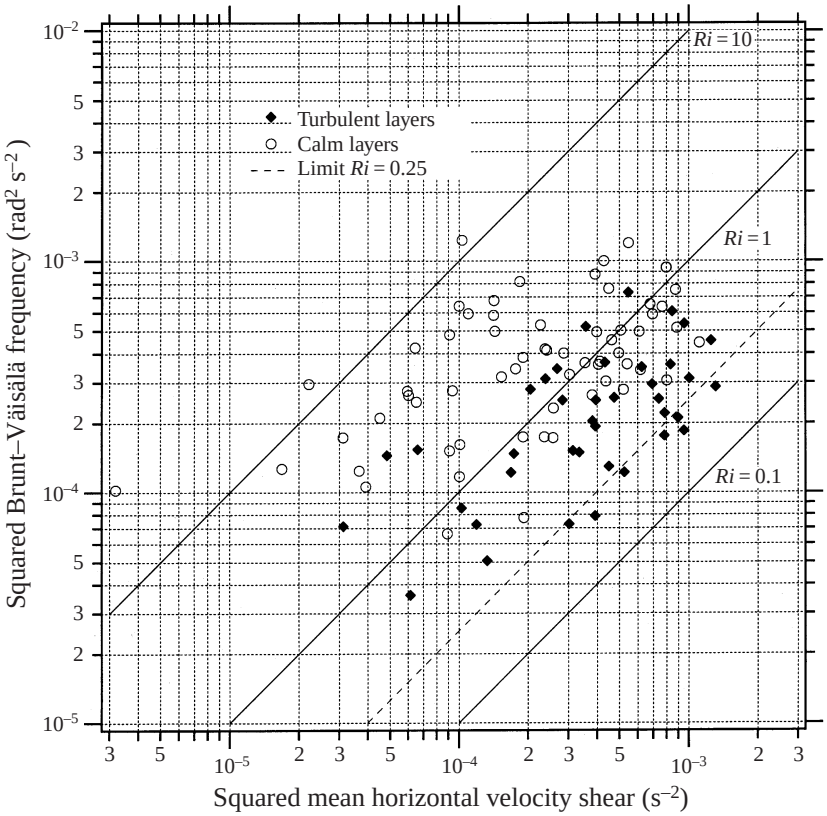

FIGURE 5. Log-log scatter plot of Brunt–Väisälä frequency N^2 versus the squared velocity shear S^2, hence yielding information about the Richardson number $Ri = N^2/S^2$. Lines corresponding to particular values of Ri (10, 1, 0.1, 0.25 dashed) have been added.

	Calm layers	Turbulent layers
N^2 (s^{-2})	4.3×10^{-4}	2.4×10^{-4}
$\overline{S}$ (s^{-1})	0.016	0.021
Ri	2.96	0.74
L_T (m)	1.54	9.12
$\overline{U'^2}$ ($m^2\,s^{-2}$)	2×10^{-3}	7.4×10^{-3}
$\overline{W'^2}$ ($m^2\,s^{-2}$)	1×10^{-3}	5.7×10^{-3}
$\overline{T'^2}$ (K^2)	8.5×10^{-5}	2×10^{-4}
$\aleph$	3.74	1.4

TABLE 5. Mean values of common parameters of calm and turbulent regimes. $\aleph$ is the anisotropy factor, defined as $\overline{U'^2}/\overline{U'^2}$.

be interpreted as the remnants of previous fully turbulent layers, according to the so-called 'fossil turbulence' theory (Gibson 1991).

The estimations of the Thorpe length are also of interest. As expected, at any given stratification parameter, turbulent layers usually show larger L_T than calm ones. These turbulent L_T are, however, much smaller than the layer depths and, as may be

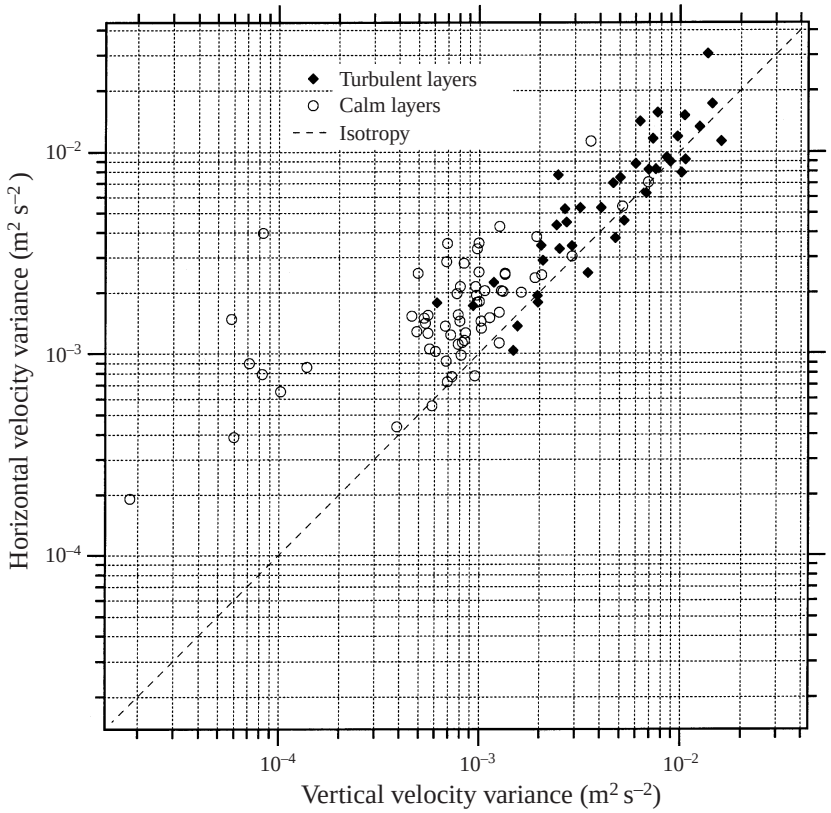

FIGURE 6. Log-log scatter plot of the horizontal velocity variance versus the vertical velocity variance. Variances are corrected for the noise contribution. Dashed line corresponds to isotropy.

expected, always weaker than L_B. This implies that, even within turbulent layers, there are not extended regions with a superadiabatic lapse rate. The vertical excursions of fluid particles, and thus turbulent scales, are much shorter than the layer depth, and this is a characteristic of turbulence within a stratified environment. Note that the same characteristics are also observed in the oceanic microstructure (Moum 1996; D. R. Caldwell, private communication 1998).

These observations, combined with those of *Ri*, suggest that turbulent layers mainly result from dynamical instability of the mesoscale field. This field often showed evidence of internal wave activity, especially during the two first flights where most of the retained turbulent layers were observed. Notice finally that, within turbulent layers, the mixing efficiency, ϵ_P/ϵ_K, lies mainly in the range 0.1–0.2, values close to those observed in the ocean.

4. Determination of PDFs of fluctuations and dependence upon the dynamical regime

In order to compare different layers, we now estimate within each one the PDFs of the *normalized* fluctuations (i.e. fluctuations divided by their standard deviation estimated within that layer) of T', W' and U'. Figure 8 shows experimental PDFs estimated within the largest calm and turbulent layers mentioned above, for these three variables. This figure shows the high similarity between distributions of a given

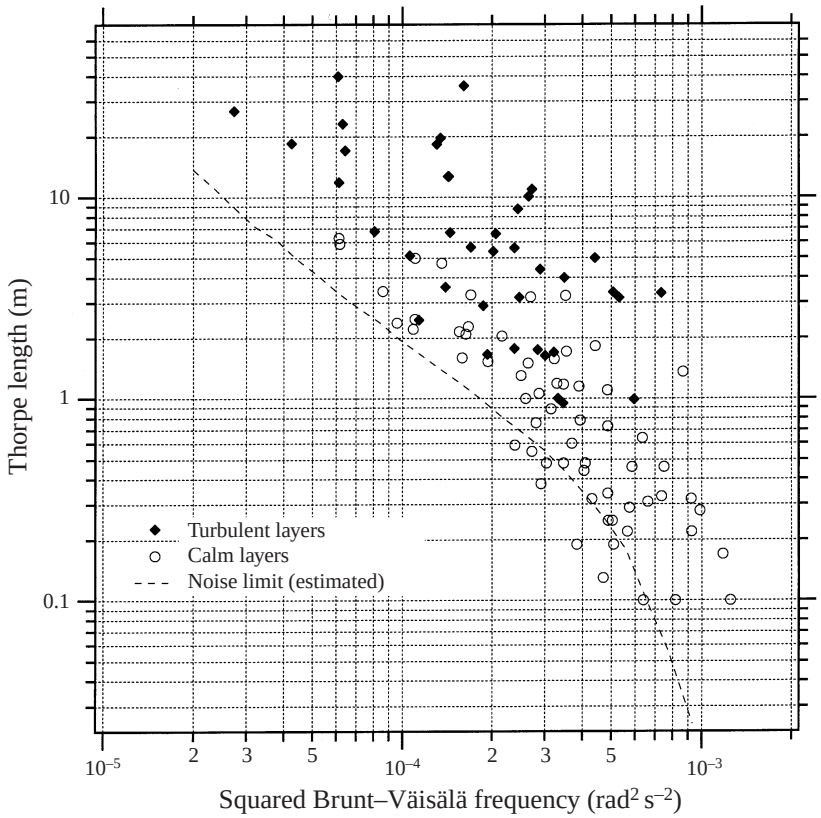

FIGURE 7. Scatter plot of Thorpe length L_T against N^2. We expect a contribution of noise to L_T, and have estimated it with a numerical simulation of a potential temperature profile with typical noise on temperature and pressure signals. Anomalously large L_T within calm layers may result from spurious local combinations of large noise and weaker $\mathrm{d}T/\mathrm{d}z$.

variable in each dynamical regime. It also shows that U' distributions differ between the two regimes, while the T' distributions appear to be very similar. Notice that while the turbulent U' and W' distributions appear similar, they apparently differ in calm conditions, thus giving more evidence of the anisotropy of the fluctuating field.

A more rigorous account of the similarities and differencies between these PDFs may be obtained using the KS test (see the Appendix). Comparisons of CDFs (cumulative density functions, see the Appendix) proceed as follows: we first choose arbitrarily one reference layer in each activity class. Then, we compare the CDFs within these two reference layers with the corresponding CDFs within all the other layers, using the KS test. Thus, the distribution of each variable within each layer is characterized by two significance levels, α^*_{-3} (comparison with the reference calm layer) and $\alpha^*_{-5/3}$ (comparison with the reference turbulent layer). As turbulent reference layers, we use a 1 km wide tropospheric layer (layer $T18$), whilst a 700 m wide stratospheric layer (layer $C16$) was used as calm regime reference layer.

Figure 9 shows for all the layers and for the three variables U', T' and W' the results of these computations as a scatter plot in a reference frame (α^*_{-3}, $\alpha^*_{-5/3}$). When considering the U' plot, two clusters of dots emerge, strictly corresponding to the two dynamical regimes. Indeed, all turbulent layers have $\alpha^*_{-5/3}$ greater than 0.05 and α^*_{-3} lower than 0.05 while the opposite occurs for calm layers. This result shows

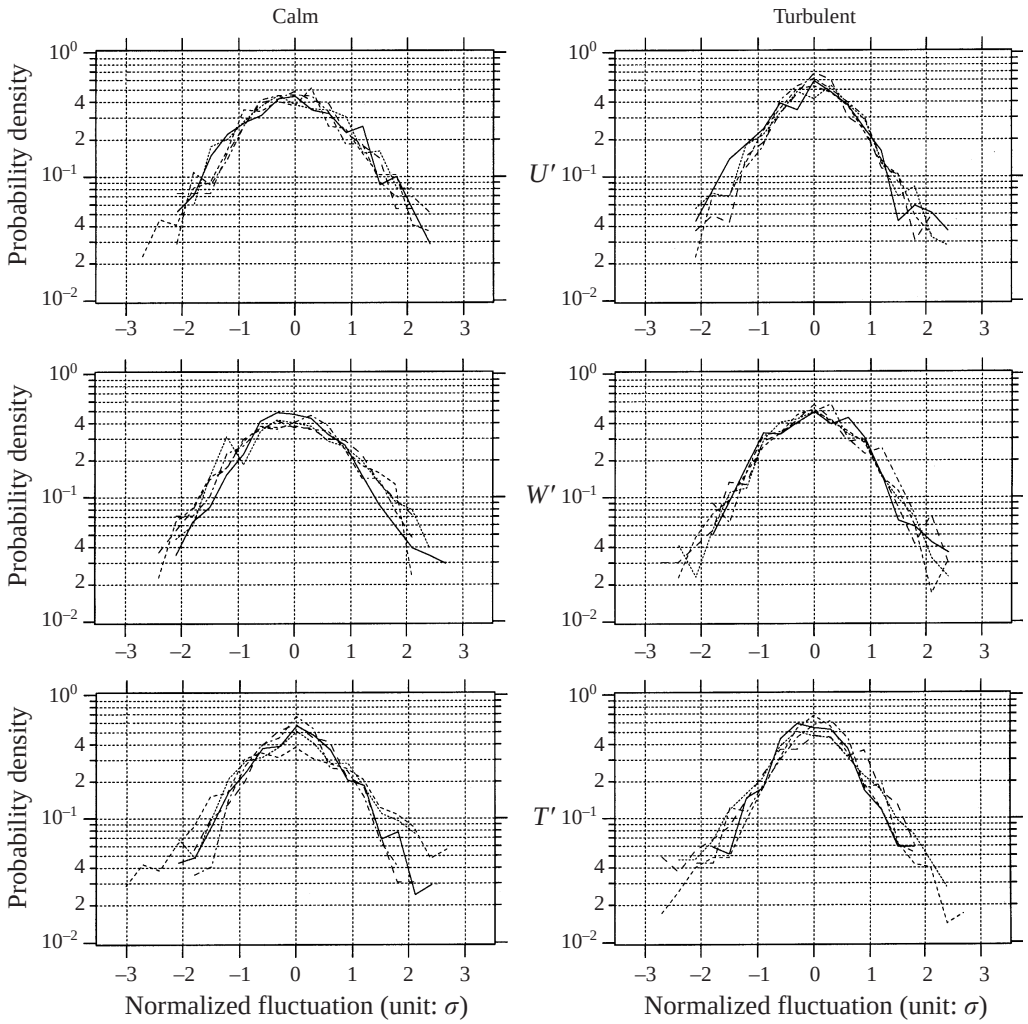

FIGURE 8. PDFs for normalized fluctuations of U', T' and W' for the five largest turbulent ($T1$, $T14$, $T16$, $T18$, $T33$) and five largest calm ($C9$, $C16$, $C18$, $C22$, $C63$) layers. Width of each bin is 0.3σ. The minimum number of occurrences per bin retained for representation is 5. The kurtosis is presented in table 4.

that all layers in a given regime (turbulent or calm) present the same distribution of normalized U' fluctuations, which differs from that in the other regime. As regards T' fluctuations, the plot shows that the distributions observed within nearly 90% of layers from both regimes do not differ significantly from the two reference distributions, as shown by the grouping of dots in the upper right quadrant. As regards W' fluctuations, the results are less clear: neither distinct clusters (as for U') nor grouping in one quadrant (as for T') occur. Nevertheless, nearly 70% of turbulent layers show distributions statistically equivalent to that of the turbulent reference layer. We present in table 6 the kurtosis of the distributions of U', T' and W' for the ten layers presented in figure 8. For those layers, the same pattern emerges as in figure 9: U' turbulent and calm distributions have different kurtosis (mean values respectively 5.14 ± 0.5 and 3.4 ± 0.2), while T' distributions present roughly the same values (mean values 6.9 ± 0.6 and 7 ± 0.8).

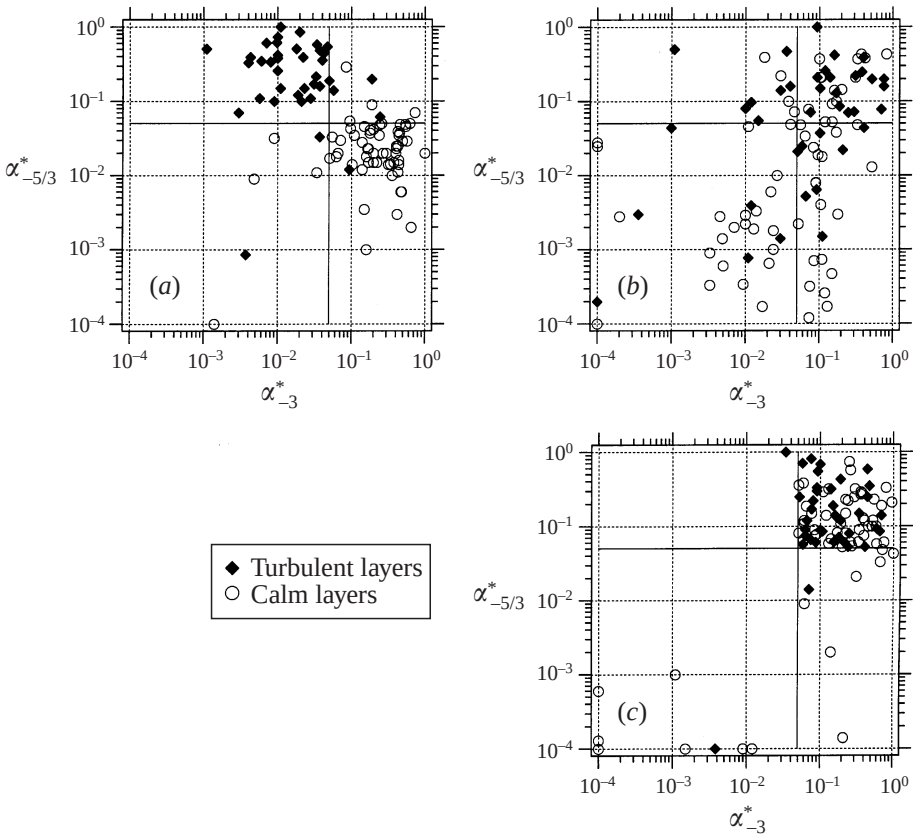

FIGURE 9. α_S distribution for (*a*) U', (*b*) W' and (*c*) T' for calm and turbulent layers represented in a $(\alpha^*_{-3}, \alpha^*_{-5/3})$ reference frame (see the text for explanation). The reference layers are the same for the three graphs (layers $T18$ and $C16$). Scales have been chosen such that dots in the upper-half of each graph represent distributions which do not significantly differ from the turbulent reference, and dots in the right-half distributions which do not significantly differ from the calm reference. Values weaker than 10^{-4} have been changed to 10^{-4} for clarity, which does not change any information: significant differences remain significant.

Layer:	$T1$	$T14$	$T16$	$T18$	$T33$	$C9$	$C16$	$C18$	$C22$	$C63$
U'	5.5	4.9	4.8	4.7	5.8	3.3	3.1	3.6	3.6	3.4
T'	7.4	6.4	6.2	7.6	6.7	6.6	5.9	7.4	6.9	8.1
W'	4.2	6.2	4.7	5.7	4.2	4.3	8.3	4.3	3.3	3.1

TABLE 6. Kurtosis of the five turbulent and five calm layers displayed in figure 8.

The observed pattern of dots in figure 9 suggest that the experimental distributions for a given parameter and regime refer to a single distribution, except for the calm W'. Such distributions may be estimated by considering the corresponding set of normalized fluctuations. We use the term composite PDFs hereafter for the experimental PDFs of such sets. These composite PDFs allow a closer analysis, especially of the tails of the distribution, as a result of the increased amount of data

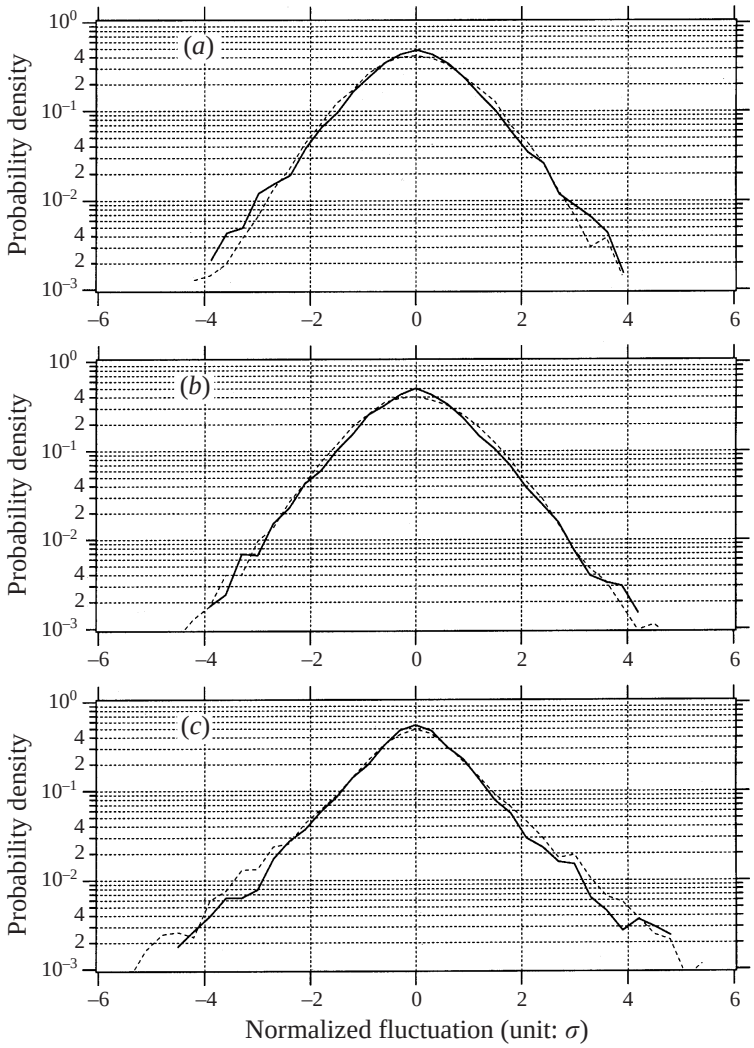

FIGURE 10. Composite PDFs of normalized fluctuations for (*a*) U', (*b*) W' and (*c*) T', corresponding to turbulent (continuous lines) and calm (dashed lines) dynamical regimes. Same representation characteristics as in figure 8.

(10 830 for turbulent PDFs, 20 010 for calm PDFs). The calm W' composite PDF is also computed, though no definite conclusions can be drawn from it.

The six composite PDFs appear in figure 10. The appearance of the composite U' PDFs in a semi-log plot strongly suggests an exponential scaling for the tails of the PDFs. The main differences between the two PDFs occur near the core of the distribution, where the calm PDF is close to Gaussian, whilst turbulent ones remain close to exponential. Further indication of the non-Gaussianity of those distributions appears when considering the kurtosis of both PDFs: we obtain for the turbulent synthetic PDF a value of 4.9 and for calm ones a value of 4.1. Recall that exact values for a Gaussian and an exponential distribution are respectively 3 and 6.

The two composite T' PDFs look very much alike. Both PDFs present extended tails that are definitely non-Gaussian. The kurtosis of turbulent and calm distributions,

Synthetic PDF:	U'_c	T'_t	T'_c	W'_t
U'_t	0.07	0.04	—	0.01
U'_c	—	—	0.09	—
T'^t	—	—	0.03	0.03

TABLE 7. Kolmogorov distances, KD, between composite CDFs of U, T and W. KD is computed for all couples of composite PDFs. The nomenclature is as follows: X_i is the synthetic PDF of X data (U', T' or W') for turbulent ($i = t$) or calm ($i = c$) layers. The choice of KD instead of α_s is explained in the text.

is, respectively, 6.88 and 6.9, thus suggesting an overall decrease slower than a pure exponential distribution.

The turbulent W' PDF also appears close to exponential and very similar to the correponding U' distribution. Its kurtosis is 4.75. As explained above, the tentative calm W' PDF is only shown here without any further comment.

Comparisons between these composite distributions may be done using the Kolmogorov distance KD (see the Appendix). We use KD here instead of the KS test because, as a result of the large amount of data collected in each set, the KS test systematically emphasizes the differences between the composite PDFs. Here, KD may be considered as a proximity index between two PDFs: the weaker it is, the closer are the two distributions we compare. Table 7 shows these KD estimates between all the PDFs pairs referring to either the same dynamical regime or the same physical parameter.

Again, the similarity of turbulent U' and W' PDFs is clear, which is an indicator of approximate isotropy of the velocity field in the spectral band considered. As expected, there is a significative difference between U' turbulent and calm distributions, while both T' distributions appear close each other.

5. Discussion

This study has been motivated by the search for distinctive statistical properties pertaining to the two most typical small-scale dynamical regimes observed in the clear, free, stable atmosphere, regimes that are also observed in other environmental stably stratified media (Holloway 1983). Though both regimes show random fluctuations of physical variables, we distinguished them as 'turbulent' or 'calm' according to the scalings, respectively $m^{-5/3}$ or m^{-3}, followed by the energy spectra versus vertical wavenumber. We estimated PDFs of fluctuations, filtered in the vertical wavelengths band (2–20 m), a spectral band influenced by one or the other dynamical regime in the troposphere and stratosphere. This spectral band is well above the dissipative scales and, presumably, below the source scales. Indeed, instabilities of mesoscale shears are usually considered as the primary source of the small-scale fluctuations considered here.

The main findings resulting from the comparisons of the PDFs of normalized fluctuations may be summarized as follows:

(i) a single PDF shape is associated with each atmospheric variable within each dynamical regime, except for the calm W' fluctuations;

(ii) calm U' PDFs significantly differ from the turbulent ones;

(iii) turbulent U' and W' PDFs are very close to each other;

(iv) calm and turbulent T' PDFs are very similar, if not identical;

(v) all these PDFs are clearly non-Gaussian: exponential shapes for the U' and W' PDFs tails, somewhat larger than exponential for T'.

These findings, except for the last, do not depend upon the precise shapes of the PDFs. Thus, they weakly depend upon possible experimental artifacts, except for the layer selection process itself. We will below first examine the influence of identified experimental shortcomings and then discuss these non-Gaussian PDFs.

5.1. *Experimental shortcomings*

The main errors are presumably linked with, (i) the effective sampling along helical paths relative to the local air flow, (ii) possible contamination of the filtered data by residual noise and (iii) the layer selection process itself.

Sampling occurs along helical paths as a result of the combination of the balloon vertical velocity, W_b, and the relative horizontal velocity, $\Delta \boldsymbol{U}$, at the gondola level. This latter has a r.m.s. modulus of about $3\,\mathrm{m\,s^{-1}}$ and, usually, slowly rotates with height (negligible rotation in the troposphere and typically 360° within 1.0–1.5 km altitude variations in the stratosphere). These observed twists of the helical paths being much larger than the wavelengths we consider here, we may assume that the effect of this rotation is negligible, at least for horizontally isotropic fields. Doing so, combined variations of ΔU and W_b within a given atmospheric layer result in both unequal sampling along variable oblique paths and a mean oblique sampling distance somewhat larger than the expected vertical sampling one. It may be anticipated that such sampling may result in an actual waveband different from the expected one. Errors, then, depend upon the isotropy or anisotropy of the fluctuating field. For an anisotropic field, the vertical decorrelation length is much shorter than the horizontal one. Thus, most of the observed variability results from the vertical displacements and most of the energy found in the actual waveband corresponds to that which would be found in an effective vertical wavelength band (2–20 m). For an isotropic field, we may represent the effective sampling as unequal along a mean constant unidirectional oblique path. Then, the effect of unequal sampling is mainly the convolution of the actual Fourier transform by some spectral window (Deeming 1975). In the present case, the expected waveband (2–20 m) is somewhat enlarged by such a convolution. Moreover, the apparent vertical wavelength band corresponds to an actual oblique wavelength band logarithmically shifted toward larger scales. Thus shift is a multiplying factor of the order of $(\Delta U^2 + W_b{}^2)^{1/2}/|W_b|$, i.e. about 1.16 during the ascents and up to 1.5 or higher during the descents. Thus, as long as the shifted band remains within the same dynamical regime, the resulting effect is mainly an increased energy of the apparent fluctuations, an effect which is eliminated by the normalization process. We must nevertheless hypothesize that PDFs of normalized fluctuations are not influenced by these *variable* wavelength shifts. This hypothesis is consistent with the very fact to compare PDFs of fluctuations within a spectral band which, in each layer, is a varying fraction of the actual $m^{-5/3}$ or m^{-3} domain. Consequently, we conclude that the identification of the actual paths with their vertical counterparts cannot introduce significant biases in the PDFs of normalized fluctuations. As an experimental proof of the above arguments, we may quote that similar PDFs have been obtained from measurements along paths with quite different oblicity, during ascending or descending parts of the flights.

Instrumental noise within the waveband considered could play some role in establishing PDF shapes. If this noise has a Gaussian distribution, the convolution with the signal distribution could account for the Gaussian pattern observed in the core of

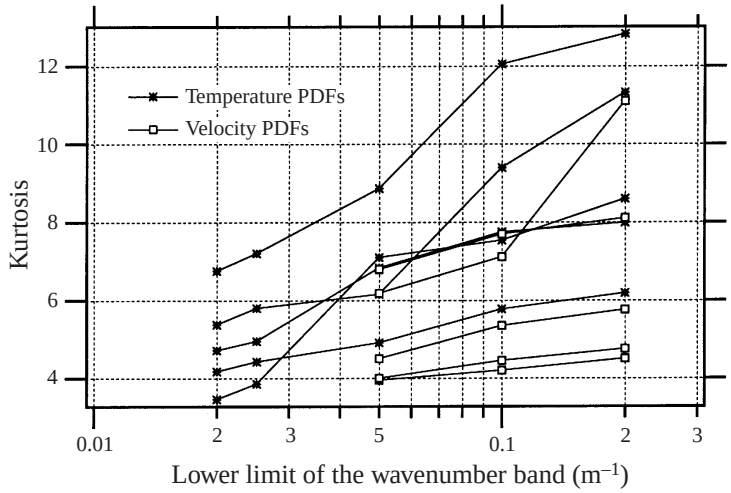

FIGURE 11. Plot of kurtosis against the largest wavelengths for different band-filtered fluctuations of temperature and horizontal velocity within turbulent layers. The shortest wavelength is always 2 m. The increase of kurtosis when the waveband goes towards small scales is considered as a proof of internal intermittency. Similar plots may be obtained within calm layers.

some PDFs (see the calm U' PDFs). Nevertheless, as stressed above, this particular shape is obtained within layers where fluctuations show quite variable energy. We may hence assert that the effect of noise is negligible, and cannot account for the shape of the core of the calm U' PDFs.

Finally, the way we selected calm and turbulent layers might affect the PDFs. First, temperature PDFs might be influenced by the fact that layers were mainly selected upon inspection of U' profiles. We mentioned that the corresponding T' fluctuations appeared less homogeneous, in both dynamical regimes. This apparent non-homogeneity in both cases could result in similar T' PDFs. Therefore, we estimated T' PDFs within seemingly homogeneous layers as regards T' signal, and obtained again the same typical shape, within apparently 'calm' or 'agitated' data sections, thus ruling out this objection.

Finally, the layer selection procedure must be thoroughly discussed. It cannot avoid some ambiguities. As already mentioned, it cannot distinguish narrow inhomogeneous sublayers from actual internal intermittency. Thus, it may influence the experimental PDF shapes. The precise extent of that influence is at present unknown, though it may be anticipated that it tends to increase the kurtosis of the resulting experimental PDFs. Nevertheless, to test if these calm subsections inside a turbulent layer may be related to real intermittency or are just an artefact of the selection procedure, we tested, for the five longest turbulent layers, the evolution of the kurtosis of the PDFs of temperature and horizontal velocity fluctuations filtered within variable wavebands. Owing to the nature of the original horizontal velocity signal, the evolution of kurtosis of velocity PDFs may only be tested when considering the shortest wavebands. Results are presented in figure 11. We see that the kurtosis increases when the spectral band reduces towards the smallest scales, as expected for intermittent signals (Frisch 1995).

Moreover, as suggested by an anonymous reviewer, we may estimate the contribution to the kurtosis computation resulting from the presence of small calm subsections interleaved with turbulent layers. Let P be the PDF of a layer with length L, P_t the PDF of the turbulent part and P_c the PDF of a calm subsection of length L_c. We

may write

$$P = \frac{L - L_c}{L} P_t + \frac{L_c}{L} P_c. \tag{5.1}$$

Let K be the total kurtosis and K_c, K_t, σ_t^2, σ_c^2 the kurtosis and variances associated to P_c and P_t; we may write

$$K = K_t \frac{1 - (L_c/L)\left[1 - K_c\sigma_c^4/K_t\sigma_t^4\right]}{\left(1 - (L_c/L)\left[1 - \sigma_c^2/\sigma_t^2\right]\right)^2}. \tag{5.2}$$

Using the reasonable hypothesis $K_c\sigma_c^4/K_t\sigma_t^4 \ll 1$, we write

$$K = K_t \frac{1 - (L_c/L)}{\left(1 - (L_c/L)\left[1 - \sigma_c^2/\sigma_t^2\right]\right)^2}. \tag{5.3}$$

Using (5.3), we may determine if the contribution of possible calm subsections may account for all of the non-Gaussianity. As an example, we consider the layer from 14.6 to 14.9 km shown in figure 2 ($T13$). A relatively quiet subsection with depth ~ 80 m appears around 14.8 km height. Here, $L = 300$ m, $L_c = 80$ m and we assume a variance ratio of 0.25. The estimated kurtosis of the velocity fluctuation PDF is 4.1. If we make the hypothesis that the actual kurtosis of the turbulent fluctuations is 3, i.e. Gaussian, then (5.3) yields a corrected kurtosis equal to 3.4, different from that measured. Hence, most of the observed kurtosis may not result only from the (eventual) statistical inhomogeneity of the layer: it corresponds, at least in part, to real intermittency of the field studied. Similar tests were conducted on other ambiguous layers and yielded similar results. We should finally add that a wrong estimate of the variance of fluctuations may lead to a biased shape of normalized fluctuation PDFs.

5.2. *The non-Gaussian PDF tails*

We first recall that 'universal' PDFs emerge for data obtained in quite different dynamical contexts. For instance, calm layers were detected in atmospheric layers nearly at rest and within the core of a strong westerly jet ($\simeq 50\,\mathrm{m\,s^{-1}}$) as well. Similarly, calm and turbulent layers have been selected with a mean stratification parameter N ranging from 7×10^{-3} to $3 \times 410^{-2}\,\mathrm{rad\,s^{-1}}$. The exponential shapes of turbulent U' and W' PDFs are noteworthy. The typical $m^{-5/3}$ scaling of the energy spectra, along with the close-to-isotropy evidence suggest *à la Kolmogorov* turbulence, i.e. that the fluctuations we consider come from a close-to-inertial subrange. Many results published on velocity PDFs in homogeneous turbulence have yielded typical Gaussian shapes. These results come from a broad range of laboratory experiments: grid-generated turbulence, isotropic (since Batchelor 1953), with cross-flow scalar gradient (Jayesh & Warhaft 1992), or even for stably stratified conditions (Thoroddsen & Van Atta 1992). Measurements in the planetary boundary layer (Van Atta & Park 1972; Katul 1994), numerical simulation with or without stratified conditions (Vincent & Meneguzzi 1991; Métais & Lesieur 1992) have led to similar results.

Since it is generally believed that the shape of velocity PDFs in homogeneous turbulence is linked with the details of the generating processes (see e.g. Frisch 1995, p. 111), the typical exponential shapes observed might be related to the main generating sources of turbulence in the stable atmosphere. Moreover, the similitude of shapes, as discussed above, suggests that all the turbulent layers observed in a vertical atmospheric profile result from similar generating processes. On the other hand, exponential shapes of PDFs are frequently interpreted as a signature of intermittency

(Yakhot 1989). One may then argue that the estimated PDFs reflect intermittency of the band-filtered fluctuations, that band lying within a close-to-inertial subrange. This assertion should be taken with the above discussed cautious remarks. While turbulent velocity data suggest isotropy, the differences between calm U' and W' PDFs – and their different energy levels as well – demonstrate anisotropy of the fluctuating field. The fact that both calm and turbulent U' PDFs present exponential tails suggests however that these tails could result from some common physical factor, that remains to be identified.

The 'identical' long-tailed shape of T' fluctuation PDFs is an important result, which deserves further comments. Non-Gaussian shapes of temperature fluctuation PDFs have already been described, in many experimental or numerical set-ups: grid-generated turbulence or pipe experiments (Gollub *et al.* 1991; Jayesh & Warhaft 1991, 1992; Guilkey *et al.* 1997), convective turbulence (Castaing *et al.* 1989), numerical simulation (Métais & Lesieur 1992; Jaberi *et al.* 1996; Ching & Tsang 1997). The grid-generated experiments mentioned above deal with the advection of temperature considered as a passive scalar, i.e. without buoyancy effects. Nevertheless, all these experiments impose a mean temperature gradient, which, in at least one experiment (Jayesh & Warhaft 1991), is a *sine qua non* condition for the emergence of non-Gaussian PDFs. For one experiment, the appearance of such shapes is linked to the value of the Reynolds number (Gollub *et al.* 1991). Pipe experiments presented in Guilkey *et al.* (1997) also stress the importance of a mean temperature gradient for the existence of long-tailed PDFs. Our results seem to support this last affirmation, in the somewhat different context of an active scalar gradient (potential temperature).

Laboratory measurements of temperature PDFs in a stably stratified turbulent flow have been published by Thoroddsen & Van Atta (1992). These authors found consistently Gaussian shapes. This major discrepancy could tentatively be explained by a major difference concerning the scale range considered in the statistics. While our results take into account only some part of a close-to-inertial subrange, it seems that all the turbulent scales, from the largest ones down to the noise level (including the Kolmogorov scale), are taken into account by Thoroddsen & Van Atta's results. Thus, the temperature fluctuation statistics they got would mainly show the statistics of the largest scales, i.e. the 'energy-containing eddies', without a detectable signature of internal intermittency. This internal intermittency does appear again in their temperature gradient statistics which show exponential tails, since differentiation (or differencing) enhances the contribution of the smallest scales. Similar analysis could explain the Gaussian PDFs obtained by Katul (1994) in the planetary boundary layer. Owing to the waveband we consider, internal intermittency appears in the fluctuation statistics themselves, and leads to the exponential tails we observe.

Métais & Lesieur (1992) present results of numerical simulations of stratified turbulence, where PDFs of both velocity and temperature are Gaussian, whilst they show non-Gaussian temperature PDFs for isotropic, non-stratified, turbulence. The authors interpreted this return to Gaussianity as the signature of the disappearance of the large-amplitude temperature signals due to the stratification. These arguments and others concerning non-Gaussianity of scalar PDFs in homogeneous turbulence are discussed by Jaberi *et al.* (1996). These authors point out that a cautious analysis of the physical conditions of each turbulent field is needed to propound any explanations of the non-Gaussianity of PDFs of turbulent fluctuations. They moreover argue that the continuous feeding of energy by the large scales seems to be a common feature of all flows presenting non-Gaussian PDFs, whilst, if there is no influx from the large scales, the PDFs collapse into Gaussian ones. In the present context, energy sources

are indeed thought to dwell above the typical scales we deal with. This could then account for the non-Gaussian shapes of the velocities PDFs we obtain, and could in turn influence the shape of T' PDFs. Note finally that with the exception of the work of Katul (1994), all those results concern turbulent flows with a thermal stratification but without a velocity shear. This fact may too account for the discrepancies observed with our results.

Stratification may play some role through (i) the existence of a mean potential temperature gradient and (ii) specific effects linked to the coupling of velocities and temperature fields via the buoyancy forces. Two arguments suggest that only point (i) should be retained. First, T' PDFs apparently do not depend upon the stratification, within the stratification range considered; notice that the same observation has already been made by Thoroddsen & Van Atta (1992), for a quite different range of values of N. Moreover, we obtain very similar T' PDFs irrespective of the dynamical regime. This apparent decoupling between temperature and velocity distributions is a rather surprising result, because both fields are linked through the buoyancy term in the momentum equation (and the conversion term in the energy equation). Such a decoupling is also present in the results of Jayesh & Warhaft (1991) and Métais & Lesieur (1992) who present non-Gaussian temperature PDFs associated with Gaussian velocity fields. Moreover, Ching & Tsang (1997) present numerical results strongly indicating that the statistical properties of a passive scalar do not depend upon the statistical properties of the velocity field. The results we present here seem to support these views, even in the case of a conservative and active scalar.

On the other hand, the extended tails of the T' PDFs with respect to those of velocity PDFs may be partly due to a particular characteristic of the temperature field in the stable atmosphere, i.e. the existence of sheets (Dalaudier *et al.* 1994*b*). These sheets are described as very strong positive temperature gradients, up to $0.3\,\mathrm{K\,m^{-1}}$, localized on significative vertical distances, typically a few metres. They have been observed throughout the discussed temperature profiles. Indeed, in the spectral space, these sheets are very wide, and produce significant amplitude events, particularly in a small-scale spectral band. Notice moreover that such relative enlargements of T' PDFs with respect to velocity PDFs have been described for velocities and temperature differences in wind-tunnel experiment (Castaing *et al.* 1990).

Our results have revealed that small-scale fluctuation statistics in the stable, free atmosphere present specific features, which seemingly differ from those obtained in laboratory measurements. They call for further research, particularly about conditional means that may help to understand both the PDFs shapes and the physical processes involved; preliminary study gives encouraging results (Alisse & Sidi 1998). Besides their intrinsic interest, this research will also help to understand the mixing processes which *in fine* remain a quite important factor for high-altitude atmospheric chemistry.

The authors thank Professor A. S. Gurvich and Dr F. Dalaudier for fruitful discussions, and an anonymous reviewer whose remarks improved considerably the first version of this work.

Appendix. Minimum length of a layer and Kolmogorov–Smirnov test

Estimations of statistical quantities – here the PDFs – from measurements raise an important question: how long must a data record be in order to get a reliable estimation of the quantity considered? This question is even more critical when

considering vertical profiles of atmospheric variables, as will be done below, i.e. measurements made along that direction where statistical homogeneity of the field variables may not *a priori* be expected. Furthermore, both *in situ* (Barat 1981) and radar (Sato & Woodman 1982) measurements revealed years ago that the depth of the alternating calm or turbulent layers may be as low as a few tens of metres. We may hence ask: what is the minimum depth a layer should have to allow statistically significant estimations of physical parameters? We may show that such a minimum length does exist, which we term 'convergence length'. It is estimated by using the Kolmogorov–Smirnov test. Given a long seemingly homogeneous section of data, we split it into subsections of increasing depths and compare their CDFs (cumulative density functions) with the CDF of the whole section. The minimum depth for which the CDFs are not significantly different is the convergence length. Note that this length is closely related to the set of lengths introduced by Lumley & Panofsky (1964) to assure the convergence of given moments. It may be in some sense considered as an extension since, by dealing with PDFs instead of mean values or variances, it gives information about all the moments, provided there is no divergence for the computation of high-order ones. This last point must be carefully verified, particularly for non-Gaussian PDFs, as shown in this article. We may show that the convergence length is dependent upon the spectral band considered. For the fluctuations in the band 2–20 m, we have estimated its value to be around 200 m.

The Kolmogorov–Smirnov (KS) test allows comparison of data series without making any *a priori* hypotheses about their distribution laws (Stephens 1970; Durbin 1973). Given two series S_1 and S_2 with respective amounts of data N_1 and N_2, the significance level of the test α_s is computed using the following formulas, where $N = (N_1 N_2)/(N_1 + N_2)$ (Stephens 1970):

$$\alpha_s = F\{(N^{1/2} + 0.12 + 0.11/N^{1/2}) \times KD\}, \tag{A 1}$$

$$F(x) = 2\sum_{k=1}^{\infty}(-1)^{k-1}\mathrm{e}^{-2k^2x^2}. \tag{A 2}$$

KD is known as the Kolmogorov distance between the two CDFs C_{N_1} and C_{N_2}:

$$KD = \sup_x |C_{N_1}(x) - C_{N_2}(x)|. \tag{A 3}$$

Clearly, α_s is a decreasing function of KD: the closer the CDFs, the larger is α_s. When α_s becomes larger than α, H_0 is considered as true. As we do not wish to give preference to the equivalence hypothesis, we will hereafter take $\alpha = 0.05$. It may be observed that the statistical distributions of the variables considered appear only through KD; thus the test does not imply any hypothesis about these distributions. This is usually considered as the main importance of the KS test (Stephens 1970; Durbin 1973).

Notice that the KS test applies rigorously to series of independent samples of random variable. Succesive samples of any hydrodynamical variable are not independent (they are not white noise). In the special case of band-filtered data, as considered below, the decorrelation length is dependent upon the bandwith considered. Strictly independent samples would thus be obtained by undersampling down to the Nyquist frequency corresponding to the largest wavelength considered. Since stationarity is assumed (correponding, here, to spatial homogeneity), such an undersampling would not change the Kolmogorov distance KD, while reducing the number of available samples within a given series. As a result, the significance level α_S (A 1), could be high

only because there is not enough information to discriminate distinct distributions. In order to take into account all the available information, we adopt below the opposite rule: the sampling rate corresponds to the shortest wavelength considered. Thus, the results of the KS test become more secure, even if applied in non fully rigorous conditions. Indeed, because of the larger amount of data, only situations corresponding to small KD are now considered non-significant by the test. On the other hand, if we used undersampled series of strictly independent samples, because of the reduced amount of data situations with high KD would have been treated as non-significant by the test. Nevertheless, to be quite cautious, α_S should be merely interpreted as a proximity index between two distributions instead of an exact confidence level. In our work, the confidence level α of the test is $\alpha = 0.05$ (Eadie *et al.* 1971).

REFERENCES

Alisse, J.-R. & Sidi, C. 1998 Non-Gaussian probability density functions of small-scale fluctuations in a stably stratified medium. In *Advances in Turbulence VII* (ed. U. Frisch), pp. 465–468. Kluwer.

Barat, J. 1981 A high resolution ionic anemometer for boundary-layer measurements. *J. Appl. Met.* **21**, 1480–1488.

Barat, J. 1982 Some characteristics of clear-air turbulence in the middle atmosphere. *J. Atmos. Sci.* **39**, 2553–2564.

Batchelor, G. K. 1953 *The Theory of Homogenous Turbulence*. Cambridge University Press.

Castaing, B., Gagne, Y. & Hopfinger, E. J. 1990 Velocity probability density functions of high Reynolds number turbulence. *Physica* D **46**, 177–200.

Castaing, B., Gunuratne, G., Heslot, F., Kadanoff, L., Libchaber, A., Thomae, S., Wu, X.-Z., Zaleski, S. & Zanetti, G. 1989 Scaling of hard thermal turbulence in Rayleigh-Bénard convection. *J. Fluid Mech.* **204**, 1–30.

Ching, E. S. 1993 Probability densities of turbulent temperature fluctuations. *Phys. Rev. Lett.* **70**, 283–286.

Ching, E. S. 1996 General formula for stationary or statistically homogeneous probability density functions. *Phys. Rev.* E **53**, 5899–5903.

Ching, E. S. & Tsang, Y. K. 1997 Passive scalar conditional statistics in a model of random advection. *Phys. Fluids* **9**, 1353–1361.

Dalaudier, F., Gurvich, A. S., Kan, V. & Sidi, C. 1994*a* Middle stratosphere temperature spectra observed with stellar scintillation and *in situ* techniques. *Adv. Space Res.* **14**, 61–64.

Dalaudier, F., Sidi, C., Crochet, M. & Vernin, J. 1994*b* Direct evidence of 'sheets' in the atmospheric temperature field. *J. Atmos. Sci.* **51**, 237–248.

Deeming, T. J. 1975 Fourier analysis with unequally-spaced data. *Astrophys. Space Sci.* **36**, 137–158.

Durbin, J. 1973 *Distribution Theory for Tests based on the Sample Distribution Function*. CBMS-NSF Regional Conference Series in Applied Mathematics. SIAM.

Eadie, W. T., Drijard, D., James, F. E., Roos, M. & Sadoulet B. 1971 *Statistical Methods in Experimental Physics*. North-Holland.

Frankignoul, C. 1974 A cautionary note on the spectral analysis of short internal wave records. *J. Geophys. Res.* **79**, 3459–3462.

Frisch, U. 1995 *Turbulence: the Legacy of A. N. Kolmogorov*. Cambridge University Press.

Gibson, C. H. 1991 Laboratory, numerical, and oceanic fossil turbulence in rotating and stratified flows. *J. Geophys. Res.* **96**, 12549–12566.

Gollub, J. P., Clarke, J., Gharib, M., Lane, B. & Mesquita, O. N. 1991 Fluctuations and transport in a stirred fluid with a mean gradient. *Phys. Rev. Lett.* **67**, 3507–3510.

Guilkey, J. E., Kerstein, A. R., McMurtry, P. A. & Klewicki, J. C. 1997 Long-tailed probability distributions in turbulent-pipe-flow mixing. *Phys. Rev.* E **56**, 1753–1758.

Hocking, W. K. 1985 Measurement of turbulent energy dissipation rates in the middle atmosphere by radar techniques: a review. *Radio Sci.* **20**, 1403–1422.

Holloway, G. 1983 A conjecture related oceanic internal waves and small-scale processes. *Atmos. Oceans* **21**, 107–122.

Jaberi, F. A., Miller, R. S., Madnia, C. K. & Givi, P. 1996 Non-Gaussian scalar statistics in homogeneous turbulence. *J. Fluid Mech.* **313**, 241–282.

Jayesh & Warhaft, Z. 1991 Probability distribution of a passive scalar in grid-generated turbulence. *Phys. Rev. Lett.* **67**, 3503–3506.

Jayesh & Warhaft, Z. 1992 Probability distribution, conditional dissipation, and transport of passive temperature fluctuations in grid-generated turbulence. *Phys. Fluids* A **4**, 2292–2307.

Katul, G. G. 1994 A model for sensible heat flux probability density function for near-neutral and slightly-stable atmospheric flows. *Boundary-Layer Met.* **71**, 1–20.

Lilly, D. K., Waco, D. E. & Adelfang, S.-I. 1974 Stratospheric mixing estimated from high-altitude turbulence measurements. *J. Appl. Met.* **13**, 488–496.

Luce, H., Crochet, M., Dalaudier, F. & Sidi, C. 1995 Interpretation of VHF ST radar vertical echoes from in situ temperature sheet observations. *Radio Sci.* **30**, 1003–1025.

Lumley, J. L. 1964 The spectrum of nearly inertial turbulence in a stably stratified fluid. *J. Atmos. Sci.* **21**, 99–102.

Lumley, J. L. & Panofsky, H. A. 1964 *The Structure of Atmospheric Turbulence*. Interscience.

Métais, O. & Lesieur, M. 1992 Spectral large-eddy simulation of isotropic and stably stratified turbulence. *J. Fluid Mech.* **239**, 157–194.

Moum, J. N. 1996 Energy-containing scales of turbulence in the ocean thermocline. *J. Geophys. Res.* **101**, 14095–14109.

Phillips, O. M. 1967 On the Bolgiano and Lumley-Shur theories of the buoyancy subrange. In *Atmospheric Turbulence and Radio Wave Propagation* (ed. A. M. Yaglom & V. I. Tatarsky). Nauka, Moscow.

Pope, S. B. 1985 PDF methods for turbulent reactive flows. *Prog. Energy Combust. Sci.* **11**, 119–192.

Pope, S. B. 1994 Lagrangian PDF methods for turbulent flows. *Ann. Rev. Fluid Mech.* **26**, 23–63.

Press, W. H., Teukolsky, S. A., Vetterling, W. T. & Flannery, B. P. 1994 *Numerical Recipes in Fortran*. Cambridge University Press.

Rabiner, L. R. & Gold, B. 1975 *Theory and Application of Digital Signal Processing*. Prentice-Hall.

Sato, T. & Woodman, R. F. 1982 Fine altitude resolution observation of stratospheric turbulent layers by the Arecibo 430 MHz radar. *J. Atmos. Sci.* **39**, 2546–2552.

Sidi, C. & Dalaudier, F. 1989 Temperature and heat flux spectra in the turbulent buoyancy subrange. *PAGEOPH* **130**, 547–569.

Sidi, C., Lefrere, J., Dalaudier, F. & Barat, J. 1988 An improved atmospheric buoyancy wave spectrum model. *J. Geophys. Res.* **93**, 774–790.

Sinai, Y. G. & Yakhot, V. 1989 Limiting probability distributions of a passive scalar in a random velocity field. *Phys. Rev. Lett.* **63**, 1962–1964.

Smith, S. A., Fritts, D. C. & VanZandt, T. E. 1987 Evidence for a saturated spectrum of atmospheric gravity waves. *J. Atmos. Sci.* **44**, 1404–1410.

Staquet, C. & Sommeria, J. 1996 Internal waves, turbulence and mixing in stratified flows: a report on Euromech Colloquium 339. *J. Fluid Mech.* **314**, 349–371.

Stephens, M. A. 1970 Use of the Kolmogorov-Smirnov, Cramér-Von Mises and relative statistics without extensive tables. *J. R. Statist. Soc.* **32**, 115–122.

Thoroddsen, S. T. & Van Atta, C. W. 1992 Exponential tails and skewness of density-gradient probability density functions in stably stratified turbulence. *J. Fluid Mech.* **244**, 547–566.

Thorpe, S. A. 1977 Turbulence and mixing in a Scottish loch. *Phil. Trans. R. Soc. Lond.* **286**, 125–181.

Van Atta, C. W. & Park, J. 1972 Statistical self-similarity and inertial subrange turbulence. In *Statistical Models and Turbulence* (ed. M. Rosenblatt & C. W. Van Atta). Lecture Notes in Physics, vol. 12, pp. 402–426. Springer.

Vincent, A. & Meneguzzi, M. 1991 The spatial structure and statistical properties of homogeneous turbulence. *J. Fluid Mech.* **225**, 1–20.

Yakhot, V. 1989 Probability distributions in high-Rayleigh-Bénard convection. *Phys. Rev. Lett.* **63**, 1965–1967.